CrossMark

Estimation of chlorophyll-*a* concentration with semi-analytical algorithms using airborne hyperspectral imagery in Nakdong river of South Korea

Eui-Ik Jeon[1] · Seong-Joo Kang[1] · Keum-Young Lee[1]

Abstract In this study, semi-analytical algorithms such as two-band and three-band models were used to estimate the chlorophyll-*a* (Chl-*a*) concentration in the turbid river using an airborne hyperspectral imagery. In order to select the optimal wavelength band to be used in the empirical equation, surface water was collected at the same time of acquisition of the aerial hyperspectral imagery. The spectral characteristic of the Chl-*a*, PC, CDOM, NAP, and phytoplankton were analyzed from by collected samples. The concentrations of PC and CDOM which affect the spectral characteristics to Chl-*a* were low and there was no change over time. So the range of wavelengths was able to broaden than the existing cases. As the result of widening the wavelength band, the two-band and three-band models were found to be higher R^2 than the results obtained by using the existing formula. Because the three-band model is more statistical significance than the two-band model, it is more appropriate to estimate the chlorophyll-*a* concentration in the turbid river. However, the Chl-*a* concentration of this study was relatively low at 45 mg/m^3, and the effect of PC and CDOM also was small. To estimate the correct Chl-*a* concentration, data such as airborne hyperspectral imagery and water sample need to be accumulated in different years and the correlation between optical properties and concentration should be thoroughly analyzed.

✉ Seong-Joo Kang
ksjdol@gmail.com

Eui-Ik Jeon
euiik0323@gmail.com

Keum-Young Lee
sweetlov2r@naver.com

[1] R&D Institute, Asia Aero Survey, Seoul, South Korea

1 Introduction

Algal blooms that may be a danger to the ecosystem occur in lakes, reservoirs and rivers due to environmental pollution around the world including South Korea [1]. Algal blooms that have occurred in South Korea are the mass propagation of cyanobacterial, affecting stable and safe supply of drinking water and having a very harmful effect on the ecosystem. There is a growing need to identify the occurrence of algal bloom promptly and remove phosphorus and floating matters, although it is also important to identify and solve the inflow of phosphorus which is the fundamental cause of algal bloom. For this reason, to monitor algal blooms periodically, an algae warning system has been implemented in South Korea; the system measures the concentration of Chl-*a* (chlorophyll-*a*) and the number of cyanobacterial cells at a total of 28 rivers and lakes at least once a week. The concentration of Chl-*a*, one of the pigments that cyanobacterial needs for photosynthesis, is an important parameter to examine the algal bloom [2, 3]. To measure the concentration, samples collected directly from certain locations are analyzed. However, as there are approximately 17,500 reservoirs and approximately 100,000 weirs including national rivers, local rivers and small rivers, it is challenging to collect samples from all locations to determine the concentration of Chl-*a*.

Therefore, studies using remote sensing that can acquire information promptly and economically targeting a wide area have been carried out. In the past, data acquired from a multispectral sensor mounted on a satellite or an aircraft

was used to monitor water quality such as algal bloom. Most multispectral sensors were used to observe visible light, NIR (Near infrared), MIR (Mid infrared) and FIR (Far infrared) and distinguish various forms of vegetables, rocks, soils, water bodies and artificial materials [4, 5]. However, the wavelength bands of multispectral sensor also have limitations as they are difficult to express complete spectral characteristics of various kinds of substances. This led to the development of a hyperspectral sensor capable of acquiring hundreds of continuous spectral bands in wider wavelength bands [6]. The developed hyperspectral sensor was mounted on satellites. However, with the development of a hyperspectral sensor that could be mounted on aircraft, studies were conducted to precisely estimate the concentration of Chl-*a* in water bodies, such as lakes and rivers, using high spatial resolution and radiometric resolution [7, 8]. There is a difficulty in applying the spectral mixture technique used in previous multispectral images as a method to estimate the concentration of Chl-*a* with hyperspectral images [9]. Therefore, studies to estimate the concretion of Chl-*a* by applying an empirical formula according to the combination of 1–3 bands in a certain wavelength band of the hyperspectral image have been carried out [10–15]. As such, various studies are being carried out to establish the optimal empirical formula to estimate the concentration of Chl-*a*, which is the standard of water quality evaluation, using airborne hyperspectral imagery obtained from water systems in various conditions. However, studies on the estimation of concentration of Chl-*a* using a hyperspectral sensor have not been sufficiently conducted in South Korea due to the lack of hyperspectral imagery data, studies regarding the atmospheric correction and geometric correction and water quality data measured at the time of acquisition of aerial hyperspectral imagery [16].

Therefore, a project aimed at analyzing the occurrence period, position, concentration and causes of algal bloom using the hyperspectral sensor has been carried out, since 2014, under the leadership of the Ministry of Environment, a government organization. The project also includes predicting and responding to the occurrence of algal bloom in advance from rivers where algal bloom occurs. As a part of the project, this study intends to determine the occurrence position and concentration of algal bloom in rivers from an airborne hyperspectral sensor. Asia Aero Survey Co., Ltd. and Ulsan National Institute of Science and Technology are participating in this study under the supervision of National Institute of Environmental Research. The Asia Aero Survey Co., Ltd. integrated spatial information and the environmental field with traditional mapping business. The company also concluded a contract with SPECIM, Finland and introduced the hyperspectral sensor so as to develop a new technology and a new business. In this study, the company engaged in mounting the hyperspectral sensor on aircraft to obtain images from Nakdong River where algal bloom occurs continuously. The Ulsan National Institute of Science and Technology collected basic field information when aerial photographs were taken and undertook the microscopic examination, biomass analysis and spectral characteristics experiment of algae from the water samples collected. And, in order to estimate the concentration of Chl-*a* from all hyperspectral imagery obtained at different times, the optimal equation for concentration estimation was determined through linear regression analysis of the concentration of Chl-*a* and the reflectance of hyperspectral imagery. In addition, the possibility to utilize airborne hyperspectral images was verified by analyzing the accuracy of the determined equation for concentration estimation.

2 Study area

For Nakdong River, one of the largest water resources in South Korea, the basin area of the main river accounts for approximately 25% of the whole national territory and its overall length is approximately 520 km. It passes through various major cities and is used as a drinking water source. Since an estuary dam was constructed in Nakdong River, the stagnation of water flow has occurred in dry seasons and factory wastes and living sewage have been discharged from large cities, thereby accelerating eutrophication due to the inflow of a great volume of nutrients and increasing the biomass of phytoplankton [17]. The target area is Changnyeong-Haman Weir on the lower Nakdong River where an observatory is operated by a government agency and the water quality is measured periodically (Fig. 1). The measurement showed that algal bloom has occurred every summer since 2014 and the water temperature in December 2015 and 2016 was higher than usual. In addition, algal bloom was found to have occurred even during winter seasons [18]. For such reason, the Changnyeong-Haman weir where a large volume of harmful blue-green algae occurred continuously every year in the downstream section of Nakdong River was considered appropriate as the study area to apply the band combination method to estimate the concentration of Chl-*a*.

3 Materials and methods

3.1 Water quality measurements

The Ulsan National Institute of Science and Technology sampled surface water using a sterilized water sample bottle and a boat and acquired information on basic water

Fig. 1 Location of study sites, Changnyeong-Haman weir on Nakdong River of South Korea
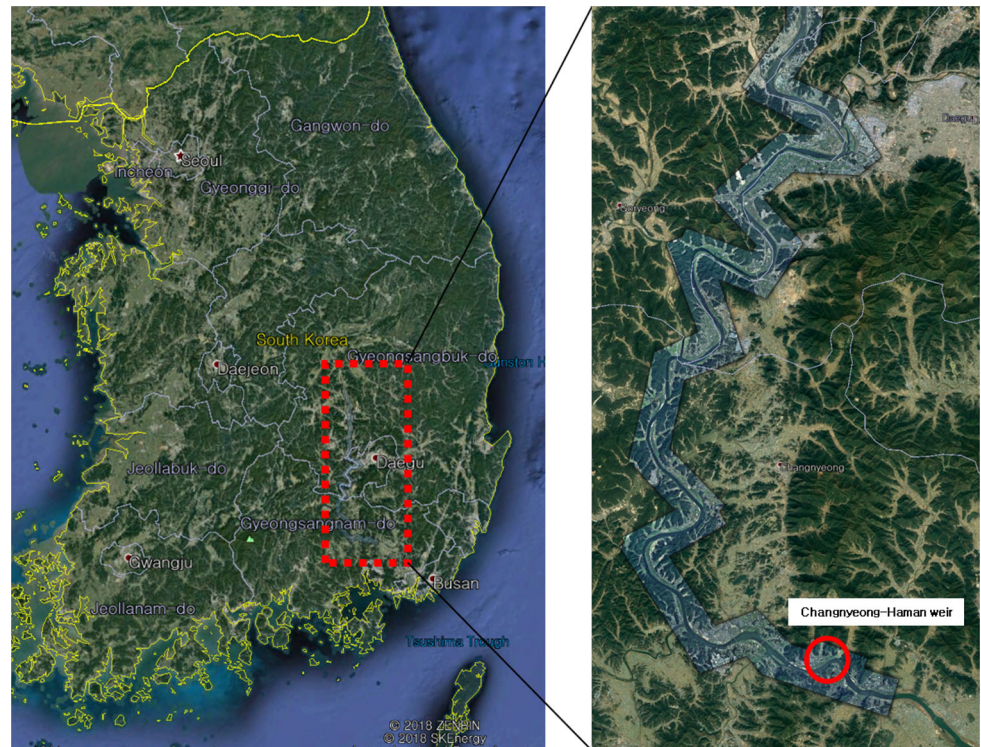
quality items such as water temperature, DO, pH and transmittance, from 15 locations near at the time when airborne hyperspectral images were taken; the institute also acquired location information using GPS (Fig. 2). The collected water samples were placed in an icebox where no light could come in and transported to the laboratory in the Ulsan National Institute of Science and Technology. To determine their spectral characteristics, the absorbance, absorption coefficients and concentrations of Chl-*a*, phycocyanin (PC), total suspended solids (TSS), colored dissolved organic matter (CDOM), phytoplankton, non-algal particles (NAP) were analyzed. To examine the spectral characteristics of these substances, the homogenization and filtration processes were undertaken and the absorbance was measured using the Cary-5000 UV–Vis–NIR spectrophotometer. The concentrations of Chl-*a* and PC and the absorption coefficients of phytoplankton and NAP can be

estimated using the absorbance of a certain wavelength band. The equation for concentration estimation and the detailed process and equations regarding the absorption coefficients are shown in [19, 20]. The concentrations of TSS are collected through the GF/F What man filter and then measured by the gravimetry.

3.2 Image acquisition and processing

SPECIM's AISA Eagle sensor was used to acquire images; the sensor was used to obtain the spectral radiance and images of the visible area and NIR area in the electromagnetic spectrum. The Eagle sensor is a push broom system where GPS/IMU is installed so that the upwelling radiance and down welling solar irradiance can be obtained with location and position information. GPS/IMU used in this study is OxTS's Survey+ and it has up to 1 cm

Fig. 2 Map of sampling stations
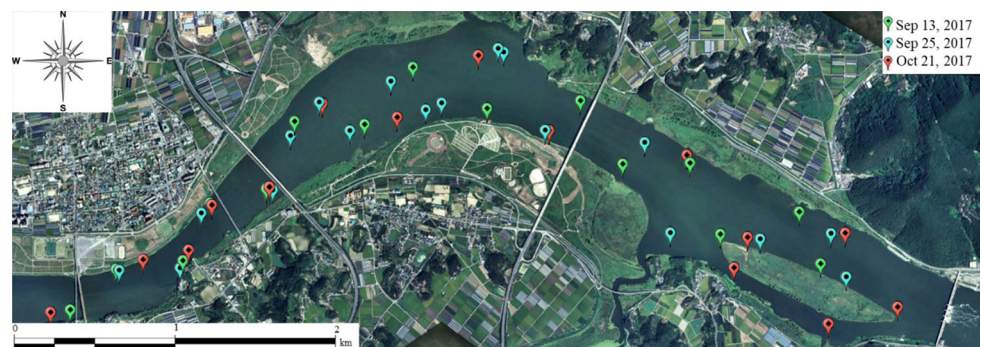
location accuracy and 0.03° (Roll, Pitch) and 0.1° (Heading) position accuracy. Approximately 200 km section from the upper area of Gumi weir to the Changnyeong-Haman weir in Nakdong River was divided into 25 areas using this sensor and 127 continuous bands having 2 m spatial resolution (wavelength range and bandwidth are 4.4 between 400 and 430 nm, 4.5 between 430 and 492 nm, 4.6 between 497 and 580 nm, 4.7 between 584 and 688 nm, 4.8 between 693 and 900 nm) were obtained at three occasions (September 13, September 25, October 21) at a flying height of 3000 m.

To obtain necessary information from airborne data, preprocessing including radiometric correction, geometric correction and atmospheric correction is necessary. Radiometric correction is a process to correct the level of radiation energy on the ground surface distorted due to the geometric relationships between the ground surface and the sensor and the response characteristics of the sensor. Geometric correction is a process to correct geometric distortion that occurs in the process of converting a 3D shape of earth into a 2D plane. For the radiometric and geometric corrections, Bore sight calibration data, raw hyperspectral image data, GPS/IMU data at the time of photographing and digital elevation models were entered and processed in CaliGeo Pro software, the exclusive preprocessing S/W of AISA Eagle sensor. Atmospheric correction is a process to eliminate atmospheric effects such as scattering, absorption and transmission from airborne hyperspectral imagery in order to calculate the reflectance of an object on the ground surface accurately. Since the atmospheric correction of hyperspectral imagery enables the acquisition of information regarding the vapor amounts of the air directly from a specific wavelength band, the atmospheric correction technique by an atmospheric model such as moderate resolution transmittance (MODTRAN) and S6 is mainly used [6]. In this study, the atmospheric correction was carried out using the ReSe's ATCOR-4 (Atmospheric & Topographic Correction for wide FOV airborne optical scanner data) based on Mod-tran-5 and information such as the vapor amounts of the air, solar zenith angle and azimuth angle, and visibility. Here, for the vapor amounts of the air, the information of 820 and 940 nm bands was used; for solar zenith angle and azimuth angle, the built-in astronomical calculator of ACTOR-4; and for the visibility, terrestrial observation data from the Korea Meteorological Administration. Since after the atmospheric correction, the spectral curve was not smooth due to the unique characteristics of the sensor and an error in the process, the distortion of information was minimized and corrected using the Savitzky–Golay smoothing model. However, a strong noise appeared in the wavelength after 760 nm that showed strong absorption by water in the NIR area; the wavelength after 760 nm could not be used. After geometric and atmospheric correction, the images were mosaicked to create the entire scene. Hyperspectral mosaic of the study area in the entire scene is shown in Fig. 3.

3.3 Semi-analytical algorithms

The photosynthetic pigments of algae absorb and use visible rays in the wavelength area between 400 and 750 nm for photosynthesis. The wavelength of light absorbed, reflected or transmitted varies according to the type of photosynthetic pigment. Generally, Chl-a absorbs the blue area (400–500 nm) and red area (620–700 nm) well among visible rays, showing a low reflectance, but shows a high reflectance in green area (500–600 nm) due to its low absorbance. And, Chl-a shows a high reflectance in 700 nm area of NIR area. When PC, TSS and CDOM, in addition to Chl-a, exist in inland water with a high turbidity level, the spectral pattern of water body changes, and such substances create an interference effects on unique spectral characteristics of Chl-a. Therefore, to estimate the concentration of Chl-a, a method to draw an empirical equation by the concentration using a specific band having less spectral interference effect by other substances and the linear regression analysis of the specific band is used. From a single band to three bands are used as independent variables in the empirical equation, and the concentration of Chl-a acquired at the time of acquiring images is used as a dependent variable [16].

A study using a certain single band such as 676 and 700 nm where a high reflectance was shown was carried out in the development of empirical equation for estimating the concentration of Chl-a from hyperspectral imagery of turbid water [21, 22]. The concentration estimation using a single band is a simple method with the linear regression techniques of the actually measured concentration of Chl-a and major wavelength. However, it is difficult to analyze the concentration of Chl-a and other factors existing in the water body using the wavelength of a single band. For this reason, the empirical equation for estimating the concentration of Chl-a using two bands and three bands in the NIR-red area was presented in order to explain the relationship between the concentration of Chl-a and the reflectance of wavelength [23, 24].

$$Chl-a \propto R_{\lambda_1}^{-1} \times R_{\lambda_2}$$

$$Chl-a \propto \left[R_{\lambda_1}^{-1} - R_{\lambda_2}^{-1} \right] \times R_{\lambda_3}$$

The presented empirical equation is a method using the two-band model and the three-band model as semi-analytical models, and each model uses the linear correlation with the band ratio and concentration that reflect the optical

Fig. 3 Hyperspectral mosaic of the study area obtained at Sep. 13, 2017
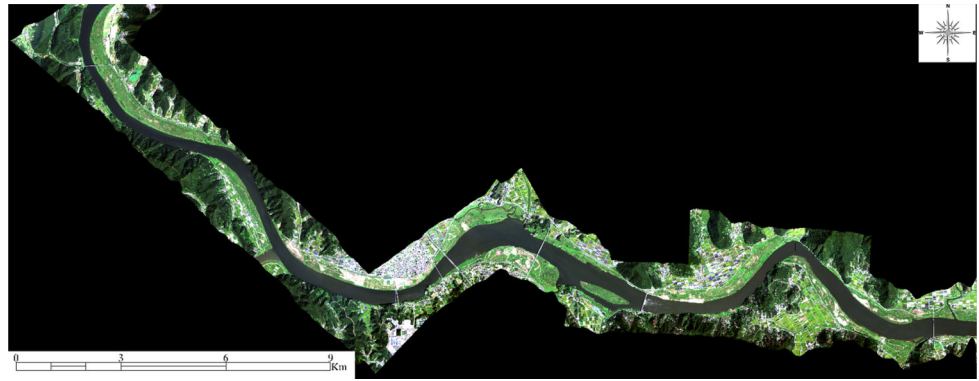
characteristics of Chl-*a* as an independent variable and a dependent variable, respectively [25]. The two-band model uses the ratio of reflectances of wavelength that shows absorption and wavelength that shows the reflection of algae factors as the concentration of Chl-*a* increases. The wavelength of between 600 and 700 nm is mainly used for λ_1; and the wavelength of between 700 and 800 nm for λ_2. The three-band model was an estimation method used to analyze Chl-*a* and pigments of vegetation on the land, but the model has been developed into a method to estimate the concentration of Chl-*a* in turbid water [24, 25]. The initial three-band model did not use the wavelength of blue area in turbid water as in the two-band model. To minimize the interference by CDOM and TSS in the Red-NIR area, the initial model used the wavelength band of over 690 and less than 730 nm beyond the absorption area of Chl-*a* for λ_2. And, λ_1 took λ_2 as close wavelength; and λ_3 used the wavelength band over 740 nm, where almost no absorption by pigments, tripton and CDOM occurred, in order to reduce a backscattering effect according to TSS change.

4 Results and discussion

4.1 In-situ water quality parameters

Table 1 shows the water temperature, DO and pH among water quality factors, and the minimum, maximum, average concentrations and standard deviation of TSS, PC and Chl-*a* obtained in the water sampling and analysis from 45 locations targeting Changnyeong-Haman weir, the downstream section of Nakdong River. At first, the average concentration of TSS was at 9.14, 10.18 and 9.78 mg/L with a variance of less than 1 mg/L, indicating the concentration was maintained almost constantly. The average concentration of PC was 0.66, 1.55 and 2.21 mg/m^3 that were low, but it increased gradually. On the contrary, the average concentration of Chl-*a* increased from 12.31 mg/m^3 on September 13–29.26 mg/m^3 on September 25, but it decreased again to 16.13 mg/m^3 on October 21, and the

overall concentration ranged between 5.21 and 44.94 mg/m^3 (Table 1).

The absorbance of Chl-*a*, PC and CDOM and the absorption coefficients of NAP and phytoplankton according to the wavelength are shown in Fig. 4. The absorption coefficients of NAP changed over time, but such change ranged between 0.1 and 0.2 on average, which is not significant. In contrast, the absorption coefficients of phytoplankton were the highest on September 25 that can be clearly distinguished from that of NAP. However, the absorption coefficients of NAP and phytoplankton were found to be the same in some sections on September 13 and October 21. The absorbance of CDOM was constant regardless of period so it could be considered almost the same. In the case of PC, its absorbance increased as its concentration increased gradually, but it had an insignificant effect on the absorption coefficients of phytoplankton. In contrast, a high absorbance of Chl-*a* was shown generally, and it changed according to a concentration change. Consequentially, the absorption coefficients of phytoplankton were found to be less affected by PC while being significantly affected by Chl-*a*.

4.2 Spectral features of river water

To obtain spectral information from a water sampling position, the spectral information of water sampling position was extracted based on the acquired location information using GPS at the time of water sampling in consideration of location errors and flexible characteristics of stream water. The spectral pattern from each water sampling location is shown at Fig. 5 for all imagery obtained at three different times.

According to the general reflectance characteristics of turbid water where algal bloom occurs, the peak appears in the ranges between 550 and 700 nm, between 620 and 650 nm, and between 690 and 710 nm and the reflectance of blue wavelength band is low. And, as the concentration of Chl-*a* increases, the reflectance on the section between 620 and 670 nm tends to decrease more significantly. In the

Table 1 Statisticsforwater quality parameter and concentration of TSS, PC, Chl-*a*

Date in 2017	Water temp. (°C)	DO (mg/L)	pH	Transparency (m)	TSS (mg/L)	PC (mg/m³)	Chl-*a* (mg/m³)
Sep. 13							
Mean	25.02	9.82	9.31	0.67	9.14	0.66	12.31
Max.	25.30	10.89	11.73	0.72	9.36	1.25	38.03
Min.	24.80	8.75	3.87	0.60	8.87	0.35	5.21
SD	0.14	0.56	1.92	0.03	0.14	0.25	7.61
Sep. 25							
Mean	24.11	14.72	12.19	0.72	10.18	1.55	29.26
Max.	23.90	16.14	13.73	0.85	10.31	1.89	44.94
Min.	24.50	13.67	9.87	0.57	10.08	1.14	16.04
SD	0.18	0.60	1.24	0.06	0.06	1.89	8.69
Oct. 21							
Mean	28.93	11.11	5.73	0.86	9.78	2.21	16.13
Max.	19.10	11.67	8.00	1.00	9.87	3.03	21.64
Min.	16.90	10.30	3.73	0.75	9.63	1.51	12.98
SD	0.51	0.37	1.29	0.06	0.07	0.42	2.44

spectral pattern of this study, it also appears in the ranges between 550 and 600, 630 and 650, and 690 and 710 nm according to the general reflectance characteristics of Chl-*a*. It is known that the section between 620 and 640 nm where a decrease in the reflectance is reduced is affected by PC. However, since the absorbance of PC was constant and the absorbance of Chl-*a* decreased in the section between 615 and 635 nm, it is considered that it was affected by Chl-*a*. And, the reflectance rapidly decreased in the section between 650 and 670 nm and this may be because the absorbance of Chl-*a* and PC increased at the ranges between 640 and 665 and 650 and 670 nm, respectively. It was also found that as the concentration of Chl-*a* is higher, the peak position in the NIR wavelength area is closer to 710 nm. When the concentrations of Chl-*a* and TSS increase, the reflectance of the whole imagery tends to increase; the result obtained on September 25 showing that the concentration of Chl-*a* increased is in accordance with this trend [26]. However, although such reflectance trend should be observed in the location where the maximum absorbance of Chl-*a* of over 0.18 was shown on September 13, the reflectances at 15 locations were constant. From this fact, it is considered that such location is an outlier; the data from such location is not used in the following experiment.

4.3 Model development

Diverse studies reflecting the characteristics of various water systems have been carried out, as the two-band model and the three-band model show different results, respectively, according to the concentrations of Chl-*a*, PC,

TSS and CDOM in the water system. Among the various water systems, the concentration of Chl-*a* showing similar characteristics to Nakdong River was estimated using the two-band model. The concentration of Chl-*a* was estimated by fixing $R_{\lambda 1}$ to 700 nm and classifying $R_{\lambda 2}$ into 592, 620 and 670 nm for the band used. R^2 ranged between 0.75 and 0.92 and RMSE ranged between 0.25 and 0.93 [13]. The correlation between the reflectance of all hyperspectral imagery obtained at different times from the two-band model and the concentration of Chl-*a* measured from the field data was analyzed with 707 nm set for $R_{\lambda 1}$ and 594.25, 622.36 and 669.55 nm set for $R_{\lambda 2}$ closely to the band used in this study. As a result, R^2 was 0.49, 0.55 and 0.32 respectively, showing a low correlation with the concentration of Chl-*a*. And, the analysis of correlation with a wavelength band used in a study that estimated the concentration of Chl-*a* using the three-band model confirmed that R^2 ranged between 0.22 and 0.43 as shown in Table 2 [14, 27]. It is considered that the reason why it was lower than R^2 in previous studies is that the target area had different concentrations of Chl-*a*, PC, CDOM and TSS and different water system conditions. To estimate the concentration of Chl-*a* with the two-band model or three-band model, it may be necessary to determine the optimal wavelength band by reflecting the optical characteristics of water body.

In the two-band model, Red-NIR wavelength band is generally used for the wavelength band. However, the analysis result in this study showed that the concentration of PC known to cause interference in the reflectance of Chl-*a* was constantly low and a change in the absorbance of PC and CDOM was insignificant. Therefore, the range
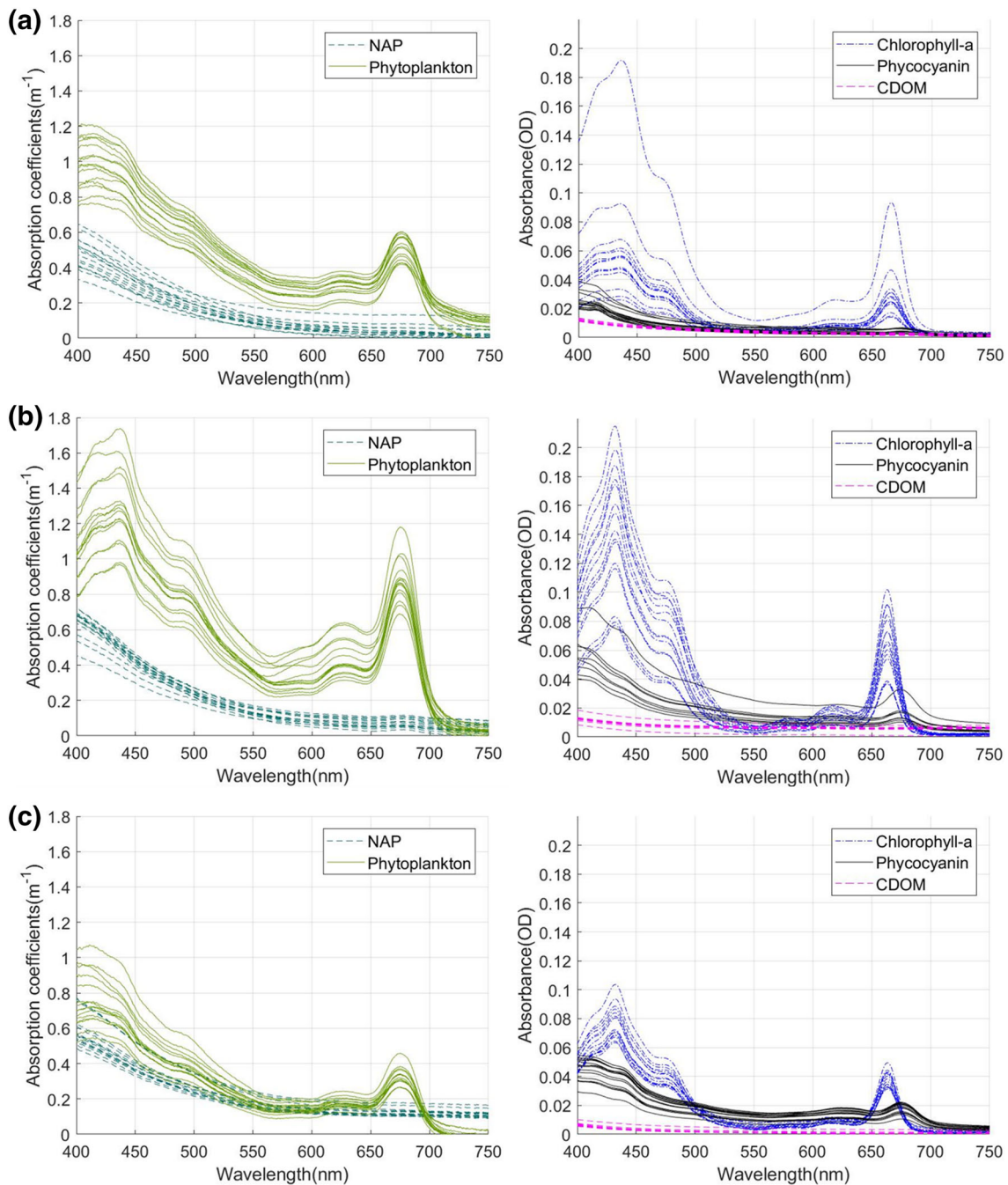
Fig. 4 Absorption coefficients of NAP, phytoplankton and absorbance of Chl-*a*, PC, CDOM. **a** Sep. 13, 2017, **b** Sep. 21, 2017, **c** Oct. 21, 2017

between 570 and 700 nm that was the whole red wavelength band was selected for the range of λ_1 and the range between 700 and 750 nm was selected for the range of λ_2 as in the previous two-band model. To find the wavelength band showing the highest correlation, λ_1 was set at 622.36 nm that showed the highest correlation among the wavelength bands selected in previous studies and λ_2 was changed. As a result, R^2 changed between 0.26 and 0.66, and R^2 was 0.66 which was the highest when λ_2 was

712.33 nm. Fixing λ_2 at 712.33 nm and changing λ_1 showed that R^2 ranged between 0.44 and 0.69 and the correlation was the highest when it was 575.61 nm. Finally, the correlation was 0.69 which was the highest when the wavelength band was 575.61 and 717.09 nm, and the RMSE of actually measured and estimated concentrations of Chl-*a* was 5.75 mg/m³ (Fig. 6). Such figures were higher than R^2 of the wavelength band used in the previous
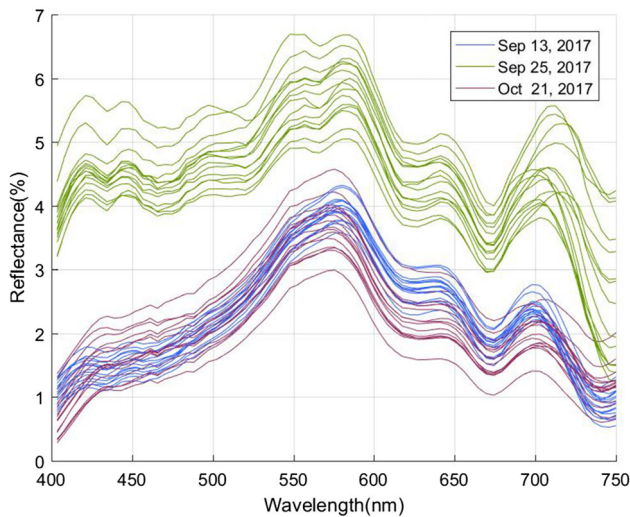
Fig. 5 Remote-sensing reflectance spectra

studies, but they are considered less statistically significant to estimate the concentration of Chl-a.

Two-band NIR-red model:

$$\text{Chl}-\text{a} = 59.62 \times R^{-1}(575.61) \times R(717.09) - 13.64$$

The ranges of λ_1, λ_2 and λ_3 to be used for the three-band model were classified into ranges between 570 and 680 nm, between 680 and 710 nm, and between 710 and 750 nm, respectively, according to the characteristics of reflectance. Their correlations were analyzed to identify the optimal wavelength band. In the first stage to identify the optimal wavelength band, λ_1 and λ_3 were fixed at 617.66 and 717.09 nm respectively and λ_2 was changed. As a result, the range of coefficient of determination was between 0.66 and 0.72, and the highest coefficient of determination was shown at 688.53 nm. In the second stage, λ_1 and λ_2 were fixed at 617.66 and 688.53 nm and λ_3 was changed. As a result, the coefficient of determination was 0.76 when λ_3 was 712.33 nm. Lastly, as a result of fixing λ_2 and λ_3 previously determined to 688.54 and 712.33 nm respectively in order determine λ_1, the coefficient of determination was 0.78 when λ_1 was 627.06 nm, showing the highest correlation with the concentration of Chl-a (Fig. 7). The three-band showed higher statistical significance than the two-band model, judging by the coefficient of determination of optimal wavelength band. The RMSE of 5.75 mg/m^3 of the three-band model was verified to be effective for estimating the approximate concentration of Chl-a in extensive areas.

Three-band NIR-red model:

Table 2 Slopes (m), intercepts (n), coefficient of determination (R^2), and root mean square error (RMSE) of the relationship "Chl-a versus model"

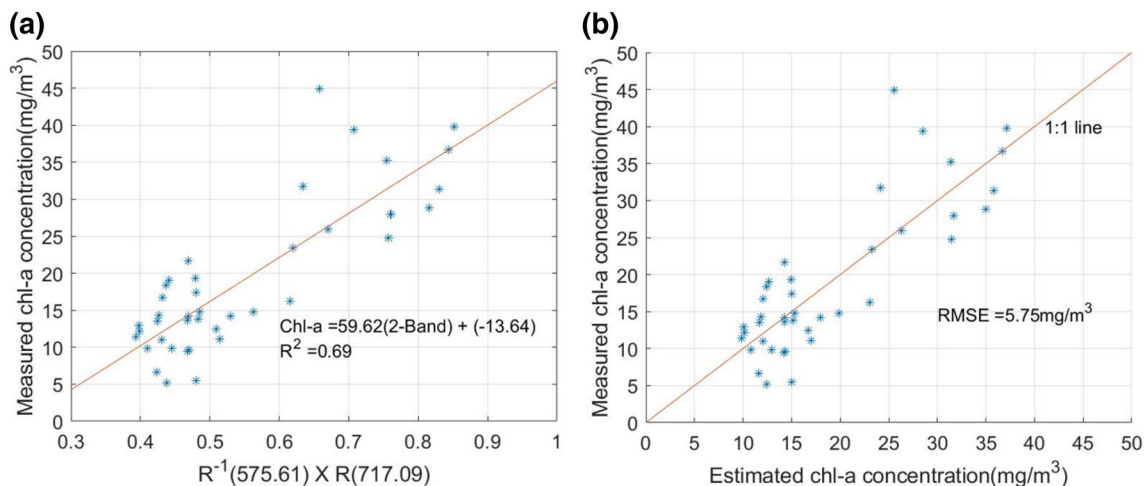| Models	m	n	R^2 (mg/m^3)	RMSE (mg/m^3)
$R_{594}^{-1} \times R_{707}$	76.34	− 32.50	0.49	7.44
$R_{622}^{-1} \times R_{707}$	71.56	− 45.87	0.55	6.94
$R_{669}^{-1} \times R_{707}$	61.48	− 57.85	0.32	8.61
$(R_{653}^{-1} - R_{691}^{-1}) \times R_{748}$	271.69	19.74	0.43	7.90
$(R_{675}^{-1} - R_{695}^{-1}) \times R_{730}$	92.89	4.79	0.22	9.25

Fig. 6 Two-band model. a Two-band model versus the measured Chl-a concentrations, b relationships between the Chl-a concentrations estimated versus measured
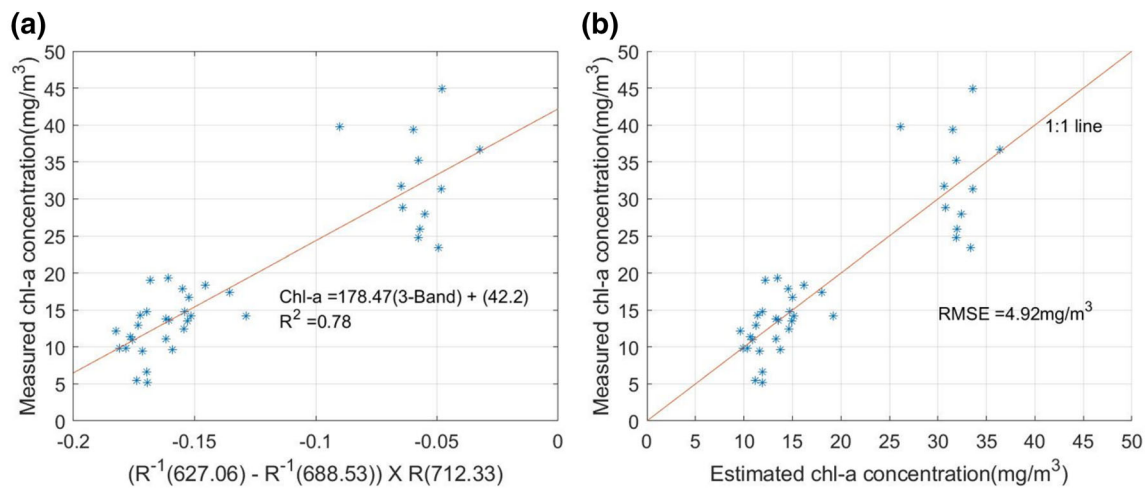
Fig. 7 Three-band model. **a** Three-band model versus the measured Chl-*a* concentrations, **b** relationships between the Chl-*a* concentrations estimated versus measured

$$\mathrm{Chl-a} = 178.47 \times \left[R^{-1}(627.06) - R^{-1}(688.53) \right] \\ \times R(712.33) + 42.20$$

5 Conclusions

In this study, the two-band model and the three-band model were applied to estimate the concentration of Chl-*a* with airborne hyperspectral imagery. In previous cases, the band model which had a high coefficient of determination ($R^2 > 0.90$) was applied, but the coefficient of determination ($R^2 < 0.55$) which was a low statistical significance level was shown. Therefore, it was considered that the combination of band combination by considering the optical characteristics of circumstances of water system in the target area in this study was essential. The concentration, absorbance and absorption coefficients of PC, TSS, CDOM, phytoplankton and NAP that caused interference in the absorption of Chl-*a* were analyzed through the instrumental analysis of the collected sample. In most studies, the 670 nm band where the interference by PC and CDOM was minimized and high absorbance of Chl-*a* appeared was mainly used for λ_1. However, the concentration of PC was almost constant regardless of period, and thus 570 and 620 nm where the absorption of Chl-*a* appeared were included. As a result, the wavelength band of the selected λ_1 was 575.61 nm in the two-band and 627.06 nm in the three-band. For the wavelength band of λ_2 of the initial three-band, the wavelength band that minimized the interference by CDOM and TSS and was close to λ_1 while being not an absorption band was used. However, 688.53 nm which was far from λ_1 was selected in consideration of the optical characteristics of this water system. Since there was no change in the concentrations of PC

and TSS that caused interference in the absorption and reflectance of Chl-*a* and only a change in the concentration of Chl-*a* occurred, it was expected that the two-band model would have a high coefficient of determination for estimating the concentration of Chl-*a*. But it showed a lower coefficient of determination ($R^2 = 0.69$) than expected. The coefficient of determination of the three-band model was 0.79, lower than the coefficient of determination ($R^2 > 0.90$) shown in other study cases, but RMSE is 5.75 mg/m^3; thus, it is considered that such model can be used to estimate the approximate concentration of Chl-*a* in large areas.

However, the following studies are necessary for precise water quality evaluation using airborne hyperspectral imagery. First, it is necessary to accumulate and analyze hyperspectral imagery at various times continuously in areas where algal bloom occurs. In the target area of this study, the concentration of Chl-*a* of over 100 mg/m^3 was recorded in 2016. This result indicates that it would be difficult to apply the band combination optimized for a relatively low concentration of less than 45 mg/m^3 at various times. Second, further studies should be conducted to estimate the concentration of other parameters affecting algal bloom. Since the concentration of Chl-*a* is not always proportionate to the number of blue-green algae cells, the concentrations of PC and TSS that are important parameters for the analysis of algal bloom should be analyzed together. However, as changes in the concentrations of PC and TSS were not significant, the experiment for estimating their concentration was not carried out. Therefore, it is necessary to closely analyze the correlation between the optical characteristics and concentrations of Chl-*a*, PC and TSS with respect to various resources showing different values of concentrations. Finally, it is necessary to find an algorithm that shows the highest accuracy in the

atmospheric correction among the preprocessing processes of airborne hyperspectral imagery. Since the reflectance of imagery may vary according to the selection of atmospheric correction algorithm, it will affect the band combination method to develop an estimation equation from the reflectance of imagery and the concentration of Chl-*a*. Therefore, it may be necessary to apply various atmospheric correction algorithms in order to improve the accuracy of estimation equation for concentrations of PC, TSS and Chl-*a* based on airborne hyperspectral imagery.

When the remote monitoring system using the airborne hyperspectral sensor is advanced in the future, it would be possible to set major pollution source areas by priority when establishing a disaster prevention implementation plan for non-point pollution sources considered as main causes of algal bloom, thus saving the investment costs for reducing non-point pollution. Such system can be also applied in evaluating the disaster prevention effects of algal bloom reduction facilities. Also, prompt response actions, tracing of pollution sources, observation of moving paths and change trend before and after the occurrence of algae bloom will be possible by measuring and monitoring the water pollution status of major rivers and lakes across the country extensively and with respect to time series in connection with the existing national automatic water quality measurement network. Remote monitoring using the airborne hyperspectral sensor is expected to be used in other environmental fields including the determination of ocean pollution by red tide, albinism, and the soil pollution by heavy metals and wastes, in addition to algal bloom.

References

1. Paerl, H. W., Fulton, R. S., Moisander, P. H., & Dyble, J. (2001). Harmful freshwater algal blooms, with an emphasis on cyanobacteria. *The Scientific World Journal, 1*, 76–113.
2. Schalles, J. F., Gitelson, A. A., Yacobi, Y. Z., & Kroenke, A. E. (1998). Estimation of chlorophyll a from time series measurements of high spectral resolution reflectance in an eutrophic lake. *Journal of Phycology, 34*(2), 383–390.
3. Richardson, L. L. (1996). Remote sensing of algal bloom dynamics. *BioScience, 46*(7), 492–501.
4. Landgrebe, D. A. (1999). Some fundamentals and methods for hyperspectral image data analysis. In *Systems and technologies for clinical diagnostics and drug discovery II* (Vol. 3603, pp. 104–114).
5. Maity, S., Mondal, I., Das, B., Mondal, A. K., & Bandyopadhyay, J. (2017). Pollution tolerance performance index for plant species using geospatial technology: Evidence from Kolaghat Thermal Plant area, West Bengal, India. *Spatial Information Research, 25*(1), 57–66.
6. Kim, S. H., Lee, K. S., Ma, J. R., & Kook, M. J. (2005). Current status of hyperspectral remote sensing: Principle, data processing techniques, and applications. *Korean Journal of Remote Sensing, 21*(4), 341–369.
7. Govender, M., Chetty, K., & Bulcock, H. (2007). A review of hyperspectral remote sensing and its application in vegetation and water resource studies. *Water Sa, 33*(2), 145–151.
8. Patra, P. P., Dubey, S. K., Trivedi, R. K., Sahu, S. K., & Rout, S. K. (2017). Estimation of chlorophyll-*a* concentration and trophic states in Nalban Lake of East Kolkata Wetland, India from Landsat 8 OLI data. *Spatial Information Research, 25*(1), 75–87.
9. Park, Y. J., Jang, H. J., Kim, Y. S., Baik, K. H., & Lee, H. S. (2014). A research on the applicability of water quality analysis using the hyperspectral sensor. *Journal of the Korean Society for Environmental Analysis, 17*(3), 113–125.
10. Gitelson, A. A., Schalles, J. F., & Hladik, C. M. (2007). Remote chlorophyll-*a* retrieval in turbid, productive estuaries: Chesapeake Bay case study. *Remote Sensing of Environment, 109*(4), 464–472.
11. Sengpiel, R. E. (2007). *Using airborne hyperspectral imagery to estimate chlorophyll a and phycocyanin in three central Indiana mesotrophic to eutrophic reservoirs.* Doctoral dissertation.
12. Moses, W. J., Gitelson, A. A., Perk, R. L., Gurlin, D., Rundquist, D. C., Leavitt, B. C., et al. (2012). Estimation of chlorophyll-*a* concentration in turbid productive waters using airborne hyperspectral data. *Water Research, 46*(4), 993–1004.
13. Olmanson, L. G., Brezonik, P. L., & Bauer, M. E. (2013). Airborne hyperspectral remote sensing to assess spatial distribution of water quality characteristics in large rivers: The Mississippi River and its tributaries in Minnesota. *Remote Sensing of Environment, 130*, 254–265.
14. Fan, C. (2014). Spectral analysis of water reflectance for hyperspectral remote sensing of water quality in estuarine water. *Journal of Geoscience and Environment Protection, 2*(2), 19–27.
15. Awad, M. (2014). Sea water chlorophyll-*a* estimation using hyperspectral images and supervised artificial neural network. *Ecological Informatics, 24*, 60–68.
16. Kim, T. W., Shin, H. S., & Suh, Y. C. (2014). Airborne hyperspectral imagery availability to estimate inland water quality parameter. *Korean Journal of Remote Sensing, 30*(1), 61–73.
17. Gwak, B. R., & Kim, I. K. (2016). Characterization of water quality in Changnyeong-Haman weir section using statistical analyses. *Journal of Korean Society of Environmental Engineers, 38*(2), 71–78.
18. Ministry of Environment. (2017). *Occurrence and response of algal-bloom.* Report, Ministry of Environment, Daejeon, Korea.
19. Dall'Olmo, G., & Gitelson, A. A. (2006). Absorption properties of dissolved and particulate matter in turbid productive inland lakes. Ocean Optics Conference, f Ocean Optics XVIII, pp. 1–15.
20. Pyo, J., Pachepsky, Y., Baek, S. S., Kwon, Y., Kim, M., Lee, H., et al. (2017). Optimizing semi-analytical algorithms for estimating chlorophyll-*a* and phycocyanin concentrations in Inland Waters in Korea. *Remote Sensing, 9*, 542.
21. Gitelson, A. (1992). The peak near 700 nm on radiance spectra of algae and water: Relationships of its magnitude and position with chlorophyll concentration. *International Journal of Remote Sensing, 13*(17), 3367–3373.
22. Dekker, A. (1993). Detection of the optical water quality parameters for eutrophic waters by high resolution remote sensing. Ph.D. Thesis, Vrije University, Amsterdam, The Netherlands.
23. Gitelson, A., Keydan, G., & Shishkin, V. (1985). Inland waters quality assessment from satellite data in visible range of the spectrum. *Soviet Remote Sensing, 6*, 28–36.
24. Dall'Olmo, G., Gitelson, A. A., & Rundquist, D. C. (2003). Towards a unified approach for remote estimation of chlorophyll-

a in both terrestrial vegetation and turbid productive waters. *Geophysical Research Letters, 30*(18), 1938.

25. Gitelson, A. A., Gritz, Y., & Merzlyak, M. N. (2003). Relationships between leaf chlorophyll content and spectral reflectance and algorithms for non-destructive chlorophyll assessment in higher plant leaves. *Journal of Plant Physiology, 160*(3), 271–282.

26. Witte, W. G., Whitlock, C. H., Usry, J. W., Morris, W. D., &Gurganus, E. A. (1981). *Laboratory measurements of physical, chemical, and optical characteristics of Lake Chicot sediment waters*. NASA technical paper.

27. Zhou, L., Roberts, D. A., Ma, W., Zhang, H., & Tang, L. (2014). Estimation of higher chlorophyll *a* concentrations using field spectral measurement and HJ-1A hyperspectral satellite data in Dianshan Lake, China. *ISPRS Journal of Photogrammetry and Remote Sensing, 88,* 41–47.